A compact X-Band ODNP spectrometer towards hyperpolarized ^{1}H spectroscopy.

Till Überrück[a], Michael Adams[a], Josef Granwehr[a,b] Bernhard Blümich[a]
[a]RWTH Aachen University, Institut für Technische und Makromolekulare Chemie, Worringerweg 2, 52074 Aachen, Germany.
[b]Forschungszentrum Jülich, Institut für Energie- und Klimaforschung – Grundlagen der Elektrochemie (IEK-9), 52425 Jülich, Germany

Abstract

The demand for compact benchtop NMR systems that can resolve chemical shift differences in the ppm to sub-ppm range is growing. However due to material and size restrictions these magnets are limited in field strength and thus in signal intensity and quality. The implementation of standard hyperpolarization techniques is a next step in an effort to boost the signal. Here we present a compact Overhauser Dynamic Nuclear Polarization (ODNP) setup with a permanent magnet that can resolve ^{1}H chemical shift differences in the ppm range. The assembly of the setup and its components are described in detail, and the functionality of the setup is demonstrated experimentally with ODNP enhanced relaxation measurements yielding a maximal enhancement of -140 for an aqueous 4-Hydroxy-TEMPO solution. Additionally, ^{1}H spectroscopic resolution and significant enhancements are demonstrated on acetic acid as a solvent.

Introduction

The use of benchtop NMR spectrometers with permanent magnets is increasing in the academic and industrial communities. Commercially available spectrometers are well suited to acquire spectra in the sub-ppm range [1,2], to perform two-dimensional correlation experiments, to monitor chemical reactions [3], and to execute pulsed field gradient experiments to study dynamic processes [4,5]. Additionally, benchtop Magnetic Resonance Imaging (MRI) scanners are available that can be applied for preclinical research or material testing [6,7]. However, the magnetic field strength of these benchtop instruments is capped by the available magnetic material and consequently limits the detection sensitivity.

It is well known that additional polarization and thus sensitivity is gained by applying hyperpolarization techniques. So far different methods have been explored with compact instruments for spectroscopic research [8]. Whereas brute force hyperpolarization is especially applied to boost signal intensity from ultra-low-field spectrometers [9,10], Para-Hydrogen Induced Polarization (PHIP) [11] or its non-reactive version Signal Amplification By Rapid Exchange (SABRE) have been successfully employed with benchtop spectrometers in the Tesla range [12–14]. In contrast, the use of Dynamic Nuclear Polarization (DNP), a more established hyperpolarization method, remains hitherto less explored with benchtop NMR. Especially the *in situ* polarization, which employs the Overhauser effect between an electron and a nuclear spin and thus is referred to as Overhauser DNP (ODNP) [15,16], is of interest in studies of liquids. It can boost signal intensity by more than two orders of magnitude while maintaining a compact design of the spectrometer compared to dissolution DNP [17] or magic angle spinning (MAS) DNP [18].

Generally, ODNP relies on the 658 times higher polarization of free electrons compared to protons, which is transferred to the surrounding nuclei mainly via dipolar exchange at ambient temperature. Due to the much higher double-quantum than zero-quantum relaxation rate in liquids the energetically higher spin state of the nucleus is populated and hence the signal is negatively amplified [20,21]. In

the literature the enhancement E_p is described by the ratio of the gyromagnetic ratios of the nucleus γ_n and electron γ_e involved, as well as the three parameters $\xi, f,$ and s [20,21].

$$E_p = 1 - \xi f s \frac{|\gamma_e|}{\gamma_n} \quad (1)$$

The coupling factor ξ accounts for the influence of the cross-relaxation rates of the system in comparison to all relaxation rates. The saturation factor s is a measure for the efficiency of the microwave (MW) pumping on the electron transitions. Last the leakage factor f describes the reduction in T_1 relaxation in the presence of the paramagnetic centers compared to the one without $T_{1,0}$.

$$f = 1 - \frac{T_1}{T_{1,0}} \quad (2)$$

About a decade ago Armstrong *et al.* [22] and Münnemann *et al.* [23] independently presented portable X-Band (8-12 GHz) ODNP setups relying on permanent magnets. Although the two publications showed signal enhancements by factors of about -100 and -50, respectively, the magnet arrays lacked field homogeneity and the ^{1}H chemical shift could not be resolved. So far spectroscopic ODNP with compact hardware has only been demonstrated in the Earth's magnetic field [19] and has more recently been demonstrated at higher fields by using Electron Paramagnetic Resonance (EPR) electromagnets [24]. However, benchtop NMR in the Tesla range relying of permanent magnets in combination with ODNP hyperpolarization, which can resolve ^{1}H chemical shift differences, has not been reported so far. In our work, we built on the work of Armstrong and Münnemann, improved their hardware concepts for X-Band ODNP hyperpolarization and integrated a freely accessible C-shaped permanent magnet into our setup that enables passive field shimming towards the level of ^{1}H spectroscopic resolution.

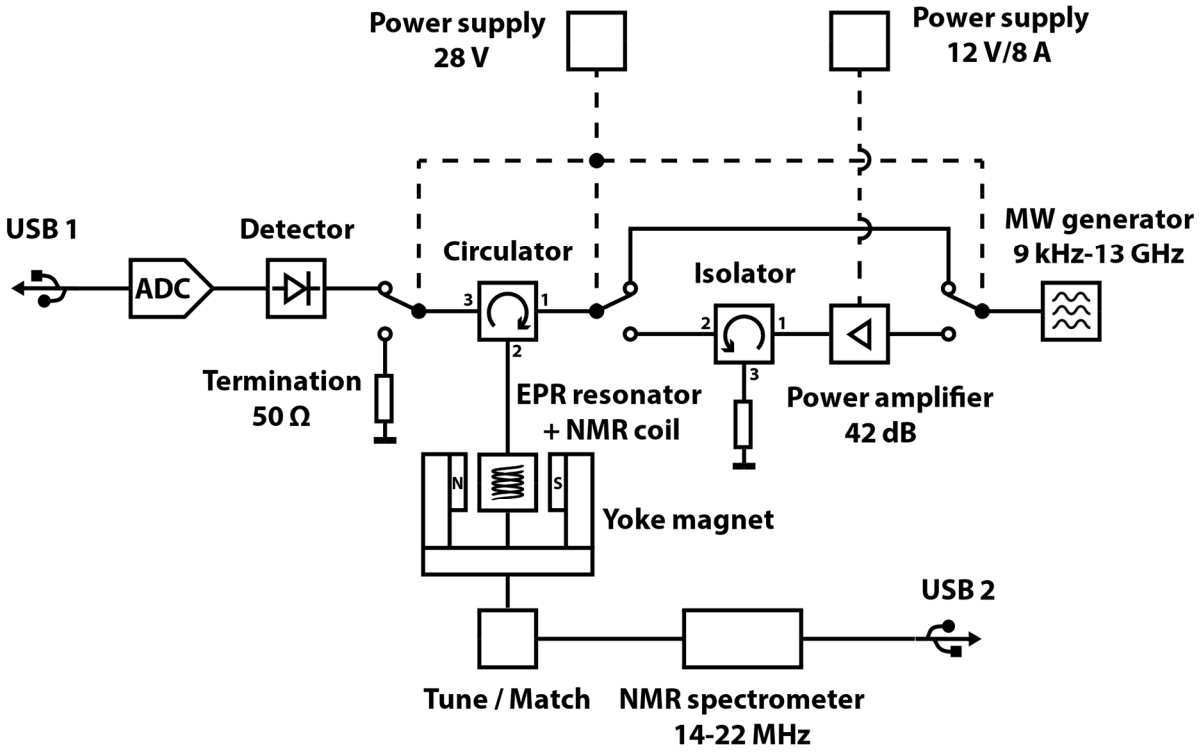

Figure 1. Wiring diagram of the X-Band ODNP setup. A freely accessible magnet contains a standard EPR resonator with an NMR saddle coil inside. The NMR signal is detected by a low-field spectrometer, and the MW irradiation is provided by an EPR circuit that can either work at low power to

determine the resonance of the cavity or at high power (42 dBm - in a 42 dBm amplification mode) to perform ODNP hyperpolarization. The assembled hardware is shown in the eSI Figures 2 and 3.

Setup

ODNP Hardware

The ODNP setup (electronic Supplementary Information (eSI) Figures 2, 3 and 4) follows a design introduced by Han *et al.* [20,22], modified to operate in a more automated fashion and to provide spectroscopic resolution. It is assembled with the components listed in Table 1 following the wiring diagram in Figure 1. The center piece of the setup is a 0.342 T C-shaped yoke magnet, which provides crude ^{1}H spectroscopic resolution. Its construction and shimming are separately presented in the subsequent section. Microwave (MW) irradiation is supplied by a generator with frequency-sweep mode option. The generator is connected to a circulator (port 1) that directs the in- and outcoming MW power to the resonator (port 2). The reflected MW power is routed via port 3 to a zero-bias detector diode. This power is rectified by the diode and converted to processable data by an analog-to-digital-converter (ADC). Measuring the reflected MW power while sweeping the frequency of the MW generator enables the determination of the resonance frequency of the EPR resonator and the adjustment of its impedance. All microwave connections are made from coaxial SMA cables (Sucoform-141, HUBER+SUHNER). To minimize power losses, the MW cable lengths were kept short by assembling the MW bridge on an integrated module.

To perform ODNP hyperpolarization experiments at elevated MW power, a MW amplifier with 42 dB gain can be inserted between the generator and the circulator. The routing of the MW power is controlled by relays, which allow automated, low loss switching of the hardware. An isolator protects the amplifier from reflected MW irradiation. A third relay protects the detector diode by routing the reflected power to a 50 Ω termination resistor during high-power MW irradiation.

For ODNP experiments an attachment box that caps the EPR resonator was made in-house. It contains the NMR tune/match circuit and a threaded rod to operate the match mechanism of the EPR resonator (eSI Figure 4a/b). A saddle coil is used to avoid blockage of the MW irradiation. Its design follows the one presented by Kaminker *et al.* [20] (eSI Figure 4c) and can hold 1 mm sample capillaries. To support the coil a 5 mm o.d. (4 mm. i.d.) sample tube is inserted inside the resonator. This also allows sample cooling with continuous air flow to counteract heating induced by MW irradiation. Communication to the MW generator and the ADC was first established via USB in Matlab 2015a. Additionally, an ODNP option, controlling the MW frequency and power, was directly embedded in a standard NMR acquisition program (Magritek Prospa V3.22).

Table 1. Hardware components of the ODNP setup (eSI Figure 2) and the individual components of the amplifier board (No. 2, eSI Figure 3).

Number	Function	Manufacturer	Product
1	MW generator	Keysight Technologies, Inc.	N5173B
2	Amplifier board	Self-manufactured	-
2-2	Relays	Teledyne Technologies, Inc.	CCR-33
2-3	Circulator	Nova Microwave™	1000CES
2-4	Detector diode	Tactron Elektronik GmbH & Co. KG	201A
2-5	Mode switch	Multi-vendor device	-
2-6	Protection relays/board	Self-manufactured	-
2-7	MW amplifier	Microwave Amplifiers Ltd.	AM53
2-7	Isolator	Nova Microwave™	1000IES
2-8	Protection switch	Multi-vendor device	-
2-9	Termination (50 Ω)	Res-Net microwave, Inc.	RFT15SFB

3	Power supplies	Voltcraft®	PPS-16005
4	Resonator	Bruker BioSpin GmbH	ER 4118X-MD5
5	Magnet	Self-manufactured	-
6	ADC	National Instruments	NI 9223
7	NMR spectrometer	Magritek	KEA²

C-shaped ^1H spectroscopy magnet

With reference to earlier work of the authors [25] a C-shaped yoke magnet was designed. The poles of the bipolar design are constructed from 37 hexagonal magnet elements (Figure 2b), each made of Sm_2Co_{17}, which maintains higher thermal stability than $Nd_2Fe_{14}B$ used in the former publication. The magnet elements are displaceable in height by M6 Allen screws at the top and bottom of the yoke to adjust the magnetic field profile. The dimensions of the magnet were designed and optimized by Finite Element Methods (FEM) using COMSOL Multiphysics 5.2 to yield a magnetic field strength of about 0.35 T, which suits the X-Band of the MW spectrum, at a gap between both poles wider than 3 cm. The final magnet specifications are listed in Table 2. Additionally, the upper part of the yoke can be slightly displaced in height to adjust the magnetic field strength to the EPR frequency at a later stage.

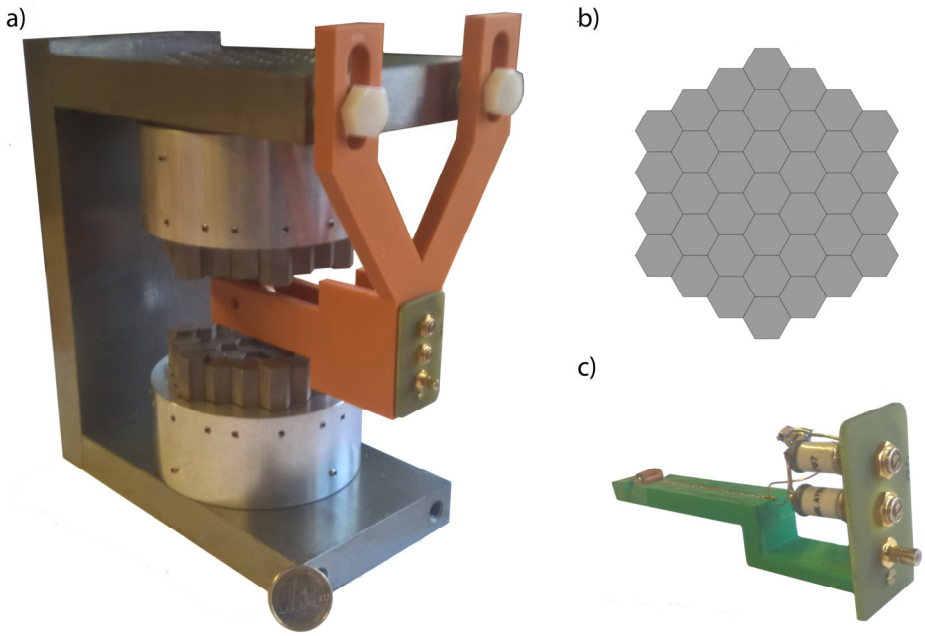

Figure 2. a) C-shaped permanent magnet working in the X-Band of the MW spectrum. A 3D printed probe (orange) is fixed inside the gap between the poles. b) Schematic drawing of the magnet array of the hexagonal poles. c) NMR-coil insert for 3D printed probe.

Table 2. Specifications of the freely accessible permanent X-Band ODNP magnet.

Parameter	Value
B_0	0.3421 T
gap	3.5 cm
material	Sm_2Co_{17}
Pole diameter	□ 8 cm
xyz-dimensions	9.0x16.4x18.8 cm³
weight	□ 15 kg

The dimensions of the hexagonal magnet elements making up the magnet poles (Figure 2b) are 13 mm in diameter and 3 cm in height for the second and third shells. In contrast to the previously published design the height of the center magnet and the first-shell magnets are reduced to 2 cm. This modification flattens the curvature of the initial magnetic field profile and hence facilitates shimming the magnet. For shimming, the displacements of the magnet elements were optimized numerically using FEM simulations in combination with the "patternsearch" algorithm of Matlab 2015a. The results of this optimization are reported in the eSI. After applying the optimized displacements, the homogeneity of the magnet was further increased with the help of three-dimensional field maps acquired with a Hall probe (F.W. Bell® 7010 Gaussmeter, accuracy 0.1 G) connected to a translation stage (ISEL® LES4).

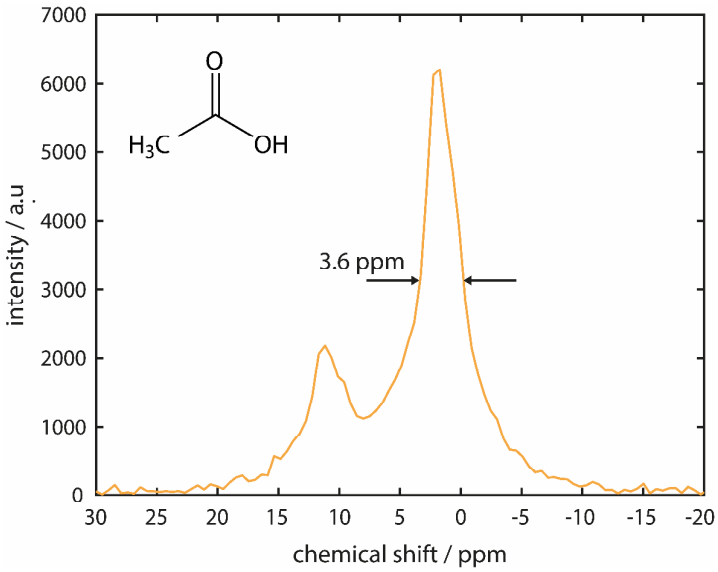

Figure 3. ^{1}H spectrum of acetic acid acquired in a 3 mm NMR tube over a length of 1.2 cm, employing the freely accessibly ODNP magnet without active shims (CH_3: 2.04 ppm, COOH: 11.73 ppm).

Subsequently an NMR probe was designed (using Autodesk Inventor Professional 2017) and 3D printed (ABS, Makerbot Replicator+) (Figure 2a/c). The probe (orange, Figure 2a) can hold various coil inserts including a tune/match circuit (Figure 2c). Using a 3 mm inner diameter solenoid coil with a length of 1.2 cm tuned to a ^{1}H frequency $\omega_0/2\pi$ of roughly 14.7 MHz and a 3 mm o.d. deionized water sample, the magnet was further shimmed on the Free Induction Decay (FID) acquired with a Magritek KEA^2 spectrometer. By displacing individual magnet elements, the length of the FID was maximized. In that way the spectral linewidth could be decreased to the ppm region, resulting in first chemical shift resolved ^{1}H spectra of simple molecules. As an example, the ^{1}H NMR spectrum of acetic acid (analytical standard, >99,8% pure, Bernd Kraft GmbH) acquired in a 3 mm sample tube is shown in Figure 3. To minimize the spectrometer deadtime and avoid ringing artifacts, the spectrum was obtained from the Fourier transform of a spin echo acquired with an echo time of 200 ms, resulting in a peak width of 3.6 ppm measured at Full Width at Half Maximum (FWHM). The spectrum is referenced to the position of the methyl peak at 2.04 ppm. According to the size – field-strength – homogeneity (SBH) ratio introduced by Parker *et al.* [26], the homogeneity of the magnet is comparable to many Halbach arrays published so far. The presented magnet shows an SBH of 0.23. The weight and size of the yoke as well as the extension of the gap prevents a higher SBH score as achieved by the Halbach spectrometers introduced by Danieli *et al.* [1].

ODNP hardware characterization

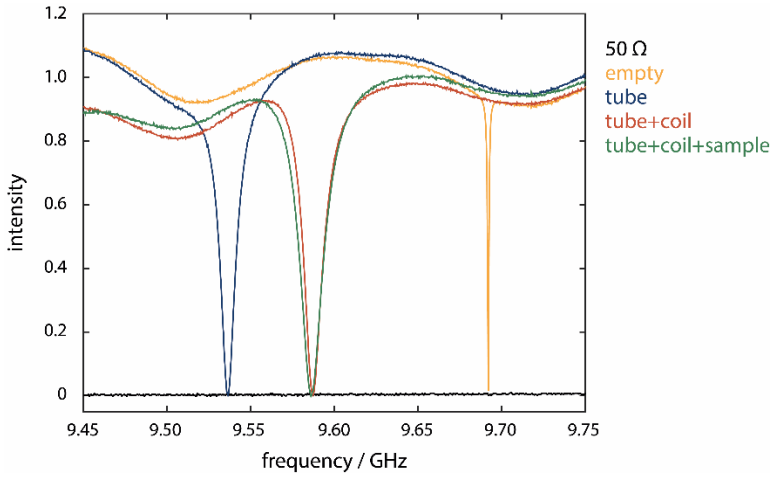

Figure 4. Resonance curve of the EPR resonator in the empty state (yellow) and with various inserts (blue: tube for cooling air; red: tube and coil; green: tube, coil and sample). The inserts shift the resonance frequency significantly and reduce the *Q*-factor of the cavity (Table 3).

To perform ODNP enhanced measurements the field of the magnet and consequently the electron and nuclear precession frequencies must match the resonance of the EPR cavity as well as the frequency of the NMR detection circuit. Whereas the NMR circuit can be easily adjusted to any desired frequency, the resonance frequency ω_0 of the commercial EPR cavity cannot be tuned. Hence the magnetic field strength and NMR frequency must be adjusted to it. Additionally, the effect of the inserts required for ODNP enhanced NMR experiments, such as glass tubing for cooling air, the NMR coil or the sample itself, on the resonance of the cavity must be evaluated. Therefore, the reflected MW power was measured as a function of frequency (Figure 4). While in the unloaded state $\omega_0/2\pi$ is at around 9.7 GHz, corresponding to the manufacturer specification, the resonance shifts to lower frequencies when the glass tube is inserted (Table 3). On the other hand, the presence of the NMR coil shifts the resonance to higher frequencies. Accompanied by these shifts the bandwidth of the resonance broadens, which results in a reduced *Q*-factor [27]

$$Q = \frac{\omega_0}{\Delta\omega_{\mathrm{FWHM}}} \tag{3}$$

where $\Delta\omega_{\mathrm{FWHM}}$ is the full width at half maximum of the resonance mode. Although a decrease in *Q* worsens the energy storage capacity of the cavity, the increased bandwidth simplifies the frequency matching of the magnet with the EPR cavity and reduces the sensitivity to external perturbations [28], which is more critical for a benchtop setup than for a stationary system.

Table 3. Resonance frequencies and quality factors of the EPR cavity in the empty state and with various inserts.

State	$\omega_0/2\pi$ / GHz	*Q*
empty	9.692	8521
tube	9.536	748
tube+coil	9.587	760
tube+coil+sample	9.586	617

Referring to the resonance with tube, coil and sample and considering the non-tunability of the EPR cavity, the magnetic field needs to be adjusted to match the NMR and EPR resonance with the specification of the resonator and hence to perform ODNP experiments. Whereas this adjustment was easily and elegantly with a pair of concentric Halbach arrays [22,23], the Halbach magnets did not provide shimming options and obtained inhomogeneities in the hundreds of ppm range. Although this inhomogeneity is no severe limitation for ODNP experiments as reported by Neudert et al. [29], we decided ion view of experiments with spectroscopic resolution to focus on shimming the magnet at the expense of the ease of field adjustment. Therefore, we had to carefully dissemble our setup to shift the poles of the C-shaped magnet apart to obtain a field strength of 0.3421 T, corresponding to a ^{1}H spin precession frequency of 14.57 MHz. With this adjustment first ODNP enhanced T_2 relaxation experiments were recorded with a 1 mm o.d. capillary filled with a 33 mM aqueous (ultrapure, 0.055 µS/cm, non-degassed) solution of 4-Hydroxy-TEMPO (Figure 5). The enhancement is clearly visible even at relatively low MW power and can reach more than two orders of magnitude upon increasing the power level. The signal enhancement approaches a value near -160 with the available MW power, which is comparable to or even slightly better than prior state-of-the-art [22,23].

The adjustment of the magnetic field worsened its homogeneity. However, in contrast to the stacked Halbach magnets, our magnet design can correct these effects by displacing individual hexagonal elements. The field homogeneity can be further improved with conventional active shims. Employing first magnetic field maps and then FIDs, the homogeneity of the magnet was adjusted again in a few iterations to the ppm level, while the absolute field strength still corresponded to an EPR resonance frequency that is within the bandwidth of the EPR cavity.

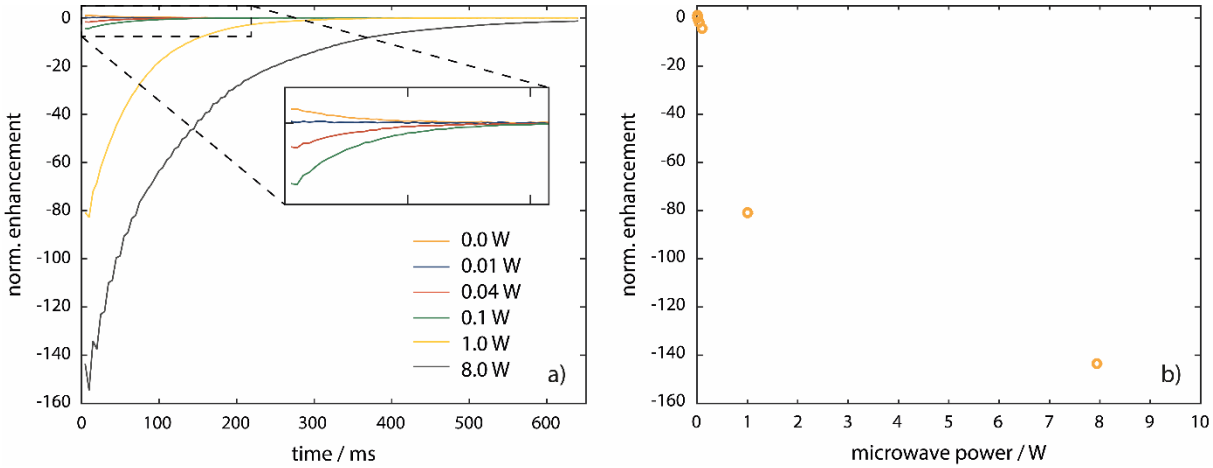

Figure 5. a) ODNP enhanced CPMG experiments of a 33 mM aqueous (ultrapure, 0.055 µS/cm) 4-Hydroxy-TEMPO sample. 128 echoes were acquired, separated by an echo time of 5 ms. Per echo 64 data points were acquired and the whole experiments was averaged over two scans. b) The hyperpolarization effect results in a signal enhancement of more than two orders of magnitude, determined at the first data point of the CPMG decay, and approaches a value close to -160 at the maximum available MW power.

ODNP ^{1}H spectroscopy

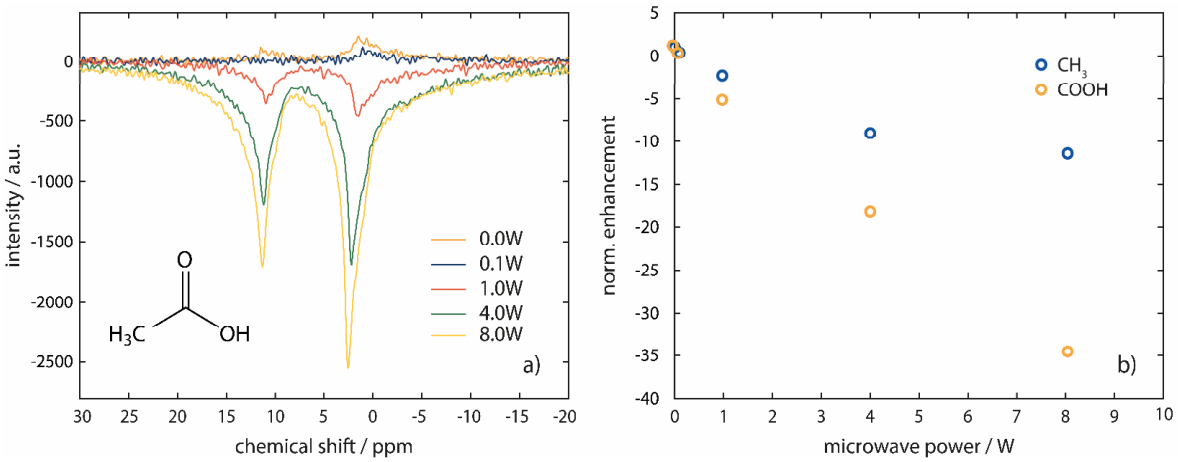

Figure 6. a) ODNP enhanced ^{1}H spectra of acetic acid doped with 33 mM 4-Hydroxy-TEMPO in a 1 mm glass capillary (CH_3: 2.04 ppm, COOH: 11.73 ppm). The peak linewidths determined at the FWHM are about 3 ppm (the exact values are listed in Table 2, eSI) b) Proton enhancement for the two resonances as a function of MW power. The carboxyl group is more strongly hyperpolarized (maximum factor of -35) than the methyl group (-11).

With the reshimmed ODNP setup the ^{1}H spectrum of an acetic acid sample (analytical standard, >99,8% pure, Bernd Kraft GmbH, non-degassed) doped with a mM amount of 4-Hydroxy-TEMPO was acquired in a 1 mm o.d. capillary at 14.58 MHz (Figure 6). The spectrum was referenced to the methyl peak at 2.04 ppm. By applying additional MW irradiation at 9.586 GHz a hyperpolarized signal was observed with a maximum enhancement of greater than -10 for both resonances. This enhancement is about an order of magnitude lower than for the relaxation measurement of the doped water sample (Fig. 5). Although the reason for this needs to be investigated further, the measurement nevertheless demonstrates, a DNP enhancement with spectroscopic resolution.

Interestingly, the peaks slightly shift during the experiments by about 1 ppm from the non-enhanced measurement to the one at 8.0 W, which is probably caused by a temperature change that can originate from two sources. The first one is the temperature dependence of the magnetic material in combination suffering a lack of temperature regulation in the laboratory. Considering the temperature coefficient of SmCo (approx. -300 ppm/K [30]), even a slight deviation in temperature of the magnetic material of about 0.003 K could cause this shift. The second may be a temperature rise of the sample due to heating induced by the interaction of the MW irradiation.

A comparison of the hyperpolarization intensities of both spectral peaks, which were determined by integrating over a fit of a Voigt line shape to each peak (Figure 6b), shows that the carboxyl peak is more intensively polarized than the methyl peak. We suggest that this is caused by the association of the spin probes with the carboxyl group due to its more hydrophilic character, which results in a stronger dipolar interaction. This hypothesis is supported by a comparison between the decrease in the longitudinal relaxation times of the functional groups due to the presence of the paramagnetic spin probes (Figure 5, eSI). The relaxation rate is increased more strongly for the carboxyl group than for the methyl group by paramagnetic relaxation enhancement effects. According to eqn. (2), the leakage factor relates to the relaxation times and results in $f = 0.22$ for the carboxyl and $f = 0.09$ for the methyl group explaining the stronger enhancement. As a high leakage factor is usually associated with a strong coupling factor [31], it can be assumed that the electron-nuclear coupling is higher, too. However, further studies are needed for a detailed analysis of the ODNP properties of doped acetic acid samples in comparison with water and other solvents.

Conclusion

In this work the design and construction of a compact X-Band ODNP spectrometer is presented. The center piece of the hardware is a freely accessible C-shaped magnet that provides chemical shift resolutions in the ppm range by just passive shimming. By adjusting the magnetic field to the specification of the EPR resonator an ODNP enhanced ^{1}H spectrum was recorded with a compact permanent magnet for the first time. The MW is switched in a semi-automatic way with the potential to offer a fully automated ODNP option at a later stage. The gap of the magnet is still sufficiently wide to introduce active electrical shims to further improve the spectral resolution. Additionally, temperature control by regulated air flow to cool the sample as well as temperature control of the magnet are necessary hardware upgrades to stabilize the equipment. Moreover, the adjustment of EPR/NMR resonance could be facilitated by constructing a tunable resonator.

Acknowledgement

The authors are grateful for the support by the Deutsche Forschungsgemeinschaft (DFG – Project: BL231/49-1) as well as the exchange networks ACalNet (funded by the Deutscher Akademischer Austauschdienst - DAAD) and the IRES program (funded by the National Science Foundation OISE, #1658652).

References

[1] E. Danieli, J. Perlo, B. Blümich, F. Casanova, Small magnets for portable NMR spectrometers, Angew. Chemie - Int. Ed. 49 (2010) 4133–4135. doi:10.1002/anie.201000221.

[2] K. Singh, B. Blümich, Trends in Analytical Chemistry NMR spectroscopy with compact instruments, Trends Anal. Chem. 83 (2016) 12–26. doi:10.1016/j.trac.2016.02.014.

[3] B. Gouilleux, B. Charrier, E. Danieli, J. Dumez, S. Akoka, F. Felpin, M. Rodriguez-zubiri, P. Giraudeau, Real-time reaction monitoring by ultrafast 2D NMRon a benchtop spectrometer, Analyst. (2015) 7854–7858. doi:10.1039/c5an01998b.

[4] G. Assemat, B. Gouilleux, D. Bouillaud, J. Farjon, V. Gilard, P. Giraudeau, M. Malet-martino, Diffusion-ordered spectroscopy on a benchtop spectrometer for drug analysis, J. Pharm. Biomed. Anal. 160 (2018) 268–275. doi:10.1016/j.jpba.2018.08.011.

[5] E.R. Mccarney, R. Dykstra, P. Galvosas, Evaluation of benchtop NMR Di ff usion Ordered Spectroscopy for small molecule mixture analysis, Magn. Reson. Imaging. 56 (2019) 103–109. doi:10.1016/j.mri.2018.09.033.

[6] E. Danieli, J. Mauler, J. Perlo, B. Blümich, F. Casanova, Mobile sensor for high resolution NMR spectroscopy and imaging, J. Magn. Reson. 198 (2009) 80–87. doi:10.1016/j.jmr.2009.01.022.

[7] S. Benders, B. Blümich, Applications of magnetic resonance imaging in chemical engineering, Phys. Sci. Rev. (2019).

[8] M.E. Halse, Perspectives for hyperpolarisation in compact NMR, TrAC - Trends Anal. Chem. 83 (2016) 76–83. doi:10.1016/j.trac.2016.05.004.

[9] M.P. Ledbetter, T. Theis, J.W. Blanchard, H. Ring, P. Ganssle, S. Appelt, B. Blu, A. Pines, D. Budker, Near-Zero-Field Nuclear Magnetic Resonance, 107601 (2011) 1–5. doi:10.1103/PhysRevLett.107.107601.

[10] S. Appelt, S. Glöggler, F.W. Häsing, U. Sieling, A. Gordji, B. Blümich, NMR spectroscopy in the milli-Tesla regime : Measurement of 1 H chemical-shift differences below the line width, Chem. Phys. Lett. 485 (2010) 217–220. doi:10.1016/j.cplett.2009.11.066.

[11] K. Jeong, S. Min, H. Chae, S.K. Namgoong, Monitoring of hydrogenation by benchtop NMR with parahydrogen-induced polarization, Magn. Reson. Chem. 57 (2018) 44–48. doi:10.1002/mrc.4791.

[12] S. Lehmkuhl, M. Wiese, L. Schubert, M. Held, M. Küppers, M. Wessling, B. Blümich, Continuous hyperpolarization with parahydrogen in a membrane reactor, 291 (2018) 8–13. doi:10.1016/j.jmr.2018.03.012.

[13] P.M. Richardson, A.J. Parrott, O. Semenova, A. Nordon, B. Duckett, M.E. Halse, SABRE hyperpolarization enables high-sensitivity 1H and 13C benchtop NMR spectroscopy, Analyst. (2018) 3442–3450. doi:10.1039/C8AN00596F.

[14] S.S. Tee, V. Digialleonardo, R. Eskandari, S. Jeong, K.L. Granlund, V. Miloushev, A.J. Poot, S. Truong, J.A. Alvarez, H.N. Aldeborgh, K.R. Keshari, Sampling Hyperpolarized Molecules Utilizing a 1 Tesla Permanent Magnetic Field, Nat. Publ. Gr. (2016) 1–6. doi:10.1038/srep32846.

[15] K.H. Hausser, D. Stehlik, Dynamic Nuclear Polarization in Liquids, Adv. Magn. Opt. Reson. 3 (1968) 79–139. doi:10.1016/B978-1-4832-3116-7.50010-2.

[16] J. Luther, P. Erik, A. Michelle, M. Timothy, Exploring the Limits of Overhauser Dynamic Nuclear Polarization (O-DNP) for Portable Magnetic Resonance Detection of Low γ Nuclei Exploring the Limits of Overhauser Dynamic Nuclear Polarization (O-DNP) for Portable Magnetic Resonance- Detection of Low γ Nuclei, 28705 (2018).

[17] J.H. Ardenkjær-Larsen, B. Fridlund, A. Gram, G. Hansson, L. Hansson, M.H. Lerche, R. Servin, M. Thaning, K. Golman, Increase in signal-to-noise ratio of>10,000 times inliquid-state NMR, Proc. Natl. Acad. Sci. 100 (2003) 10158–10163.

[18] L.R. Becerra, G.J. Gerfen, R.J. Temkin, D.J. Singel, R.G. Griffin, Dynamic nuclear polarization with a cyclotron resonance maser at 5 T, Phys. Rev. Lett. 71 (1993) 3561–3564.

[19] M.E. Halse, P.T. Callaghan, A dynamic nuclear polarization strategy for multi-dimensional Earth's field NMR spectroscopy, J. Magn. Reson. 195 (2008) 162–168. doi:10.1016/j.jmr.2008.09.007.

[20] I. Kaminker, R. Barnes, S. Han, Overhauser Dynamic Nuclear Polarization Studies on Local Water Dynamics, in: Methods Enzymol., 1st ed., Elsevier Inc., 2015: pp. 457–483. doi:10.1016/bs.mie.2015.06.040.

[21] J.R. Biller, R. Barnes, S. Han, Perspective of Overhauser dynamic nuclear polarization for the study of soft materials, Curr. Opin. Colloid Interface Sci. 33 (2018) 72–85. doi:10.1016/j.cocis.2018.02.007.

[22] B.D. Armstrong, M.D. Lingwood, E.R. McCarney, E.R. Brown, P. Blümler, S. Han, Portable X-band system for solution state dynamic nuclear polarization, J. Magn. Reson. 191 (2008) 273–281. doi:10.1016/j.jmr.2008.01.004.

[23] K. Münnemann, C. Bauer, J. Schmiedeskamp, H.W. Spiess, A Mobile DNP Polarizer for Clinical Applications, (2008) 321–330. doi:10.1007/s00723-008-0130-8.

[24] N. Enkin, G. Liu, I. Tkach, M. Bennati, High DNP efficiency of TEMPONE radicals in liquid toluene at low concentrations, Phys. Chem. Chem. Phys. 16 (2014) 8795–8800. doi:10.1039/c4cp00854e.

[25] T. Überrück, B. Blümich, Variable magnet arrays to passively shim compact permanent-yoke magnets, 298 (2019) 77–84. doi:10.1016/j.jmr.2018.11.011.

[26] A.J. Parker, W. Zia, C.W.G. Rehorn, B. Blümich, Shimming Halbach magnets utilizing genetic algorithms to profit from material imperfections, J. Magn. Reson. 265 (2016) 83–89. doi:10.1016/j.jmr.2016.01.014.

[27] J.A. Weil, J.R. Bolton, Electron Paramagnetic Resonance, John Wiley & Sons, Inc., Hoboken, NJ, USA, 2006. doi:10.1002/0470084987.

[28] J. Granwehr, Multiplicative or t1 Noise in NMR Spectroscopy, Appl. Magn. Reson. 32 (2007) 113–156. doi:10.1007/s00723-007-0006-3.

[29] F. Inhomogeneity, O. Neudert, D. Germanovich, W. Spiess, C. Bauer, P. Blu, Overhauser DNP and EPR in a Mobile Setup : Influence, (2012) 149–165. doi:10.1007/s00723-012-0347-4.

[30] E. Danieli, J. Perlo, B. Blümich, F. Casanova, Highly stable and finely tuned magnetic fields generated by permanent magnet assemblies, Phys. Rev. Lett. 110 (2013) 1–5. doi:10.1103/PhysRevLett.110.180801.

[31] J.M. Franck, A. Pavlova, J.A. Scott, S. Han, Quantitative cw Overhauser effect dynamic nuclear polarization for the analysis of local water dynamics, Prog. Nucl. Magn. Reson. Spectrosc. 74 (2013) 33–56. doi:10.1016/j.pnmrs.2013.06.001.